Chapter 6

Comparison with Experiment

DIRECT COMPARISONS of the toroidal nonlinear simulations with experiment are presented in this chapter. Recent comparisons between experiment and a transport model based on simulations with our toroidal gyrofluid code and linear fully kinetic calculations have shown good agreement in the core ($r/a < 0.85$) of L-mode type discharges [DORLAND *et al.*, 1994b; KOTSCHENREUTHER *et al.*, 1994a]. These comparisons used an interpolation formula for χ_i, parameterized to fit our toroidal gyrofluid simulation results with adiabatic electrons. This formula also uses an interpolation formula for the marginal L_{Ti}/R found from linear fully kinetic calculations with adiabatic electrons. (As discussed in Section 5.4, a critical L_{Ti}/R does not always rigorously exist with nonadiabatic electrons, but threshold like behavior may still occur in many cases.) This fit to χ_i was then used in a predictive power balance code to predict temperature profiles, and T_i and χ_i from the fit (using the predicted T_i) were compared with experiment. Many L-mode ($\sim$ 50) shots were simulated in this manner, finding encouraging agreement. In this Chapter, a simpler, more direct approach is taken. Measured temperature and density profiles are used as inputs for the toroidal gyrofluid simulations with trapped electrons, and the resulting χ_i's and χ_e's are compared with those inferred from power balance. This comparison is presented here to roughly demonstrate where we stand, and should be considered qualitative.

The specific shot chosen is TFTR L-mode #65018, and the input parameters are taken from SNAP try 3. This shot is very similar to #65012 in [SCOTT *et al.*, 1993]. The primary ion species is deuterium, heated by 14MW of deuterium neutral beam injection. The major radius is $R_0 = 245$cm, the minor radius is $a = 80$cm, and the toroidal field strength on axis is $B_0 = 4.8$T. The Shafranov shift is not terribly large, 11.8cm at the magnetic axis, so the simulations use concentric circular flux surface geometry. In this shot the impurity concentration is small, $Z_{\text{eff}} = 1.73$. At $r = 0$, the beam density is $n_b/n_e = 0.15$, and the hydrogen and carbon impurity densities are $n_H/n_e = 0.071$ and $n_C/n_e = 0.024$, with carbon making largest contribution to Z_{eff} and to the impurity charge density. Metal impurities are negligible. The calculated beam density decreases monotonically towards the edge. Because of this relatively low impurity and beam concentration, in the simulations impurities and beams are neglected. The measured Z_{eff} (assumed independent of minor radius) is used to calculate the electron-ion collision frequency.

The profiles taken from SNAP are shown in Figs. 6.1-6.3. Since $\eta_i = L_{ni}/L_{Ti}$ varies from 1.5 to 4, the turbulence in this shot is driven by the toroidal ITG mode. Several small flux tube simulations, centered at different r/a, are run using the local measured parameters as input. The chosen numerical parameters vary slightly with the physical parameters to ensure adequate resolution. In particular, the simulations find a strong q dependence of the peak in the nonlinear fluctuation spectrum. At the edge where q is large, the spectrum peaks at lower k_θ, so larger simulation domains are required to resolve these long wavelengths. The results from these nonlinear simulations are shown in Fig. 6.4 and compared against χ_i and χ_e from power balance. Also shown is the predicted χ_i from [Biglari *et al.*, 1989], $\chi_i = [k_\theta \rho_i q(1+\eta_i)/(\tau \hat{s})]\, \rho_i^2 v_{ti}/L_n$. Since $k_\theta\rho_i$ is not determined from this theory, $k_\theta\rho_i = 0.2$ is used. Using $k_\theta\rho_i$ found from the simulations would exacerbate the difference between this theory and experiment, since $k_\theta\rho_i$ from the simulations decreases with increasing minor radius. In the core ($r/a < 0.2$), all modes are stable for the measured parameters, but just barely; a small increase in ∇T_i would destabilize the toroidal ITG mode and give a small χ_i. (This shot had sawteeth, which might be complicating things in this region, since the $q = 1$ surface is at about $r/a = 0.25$.)

There is a tendency for the predicted χ from the simulations, χ^{sim}, to over- and undershoot χ^{PB} calculated from power balance. This is related to the dependence of the χ's on ∇T, and the fact that the measured ∇T, as a gradient, is more susceptible to experimental uncertainties than local quantities. The experimentally

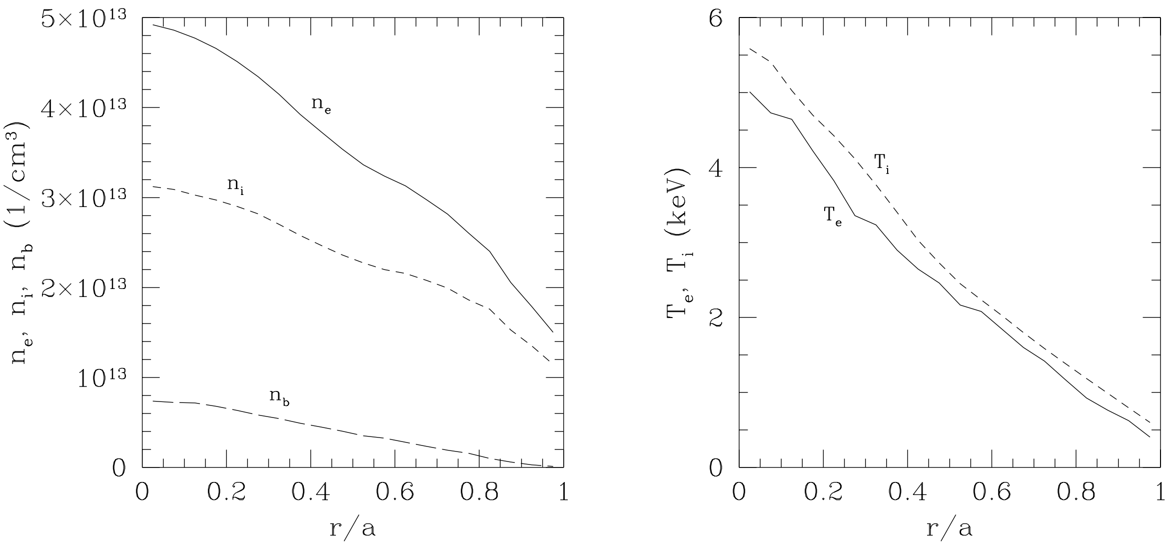

Figure 6.1: Measured electron (solid) and ion (dashed) density and temperature profiles, and beam density (long dashes) for #65018 from SNAP.

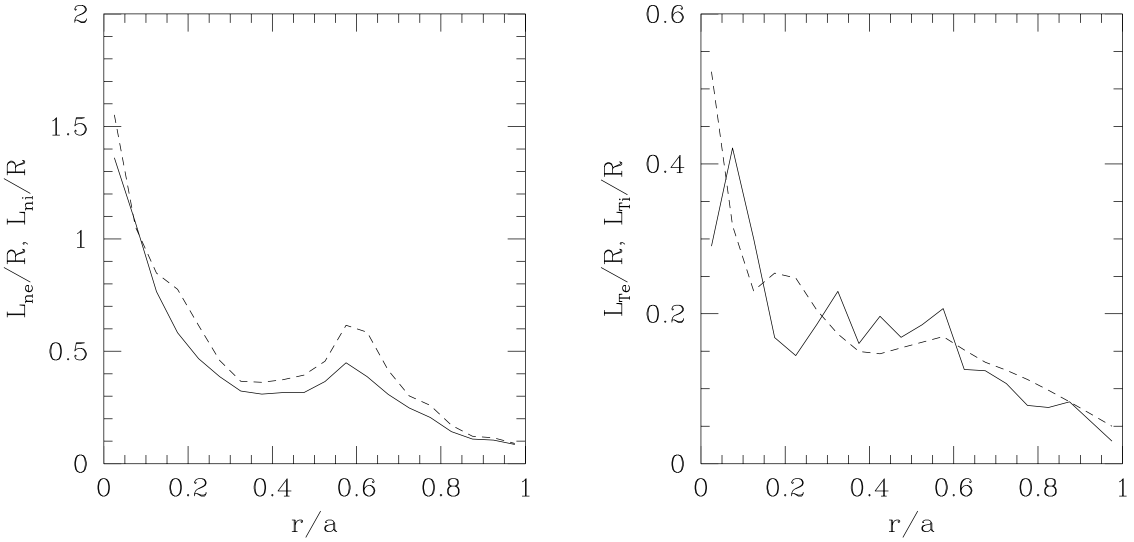

Figure 6.2: Electron (solid) and ion (dashed) density and temperature scale lengths.

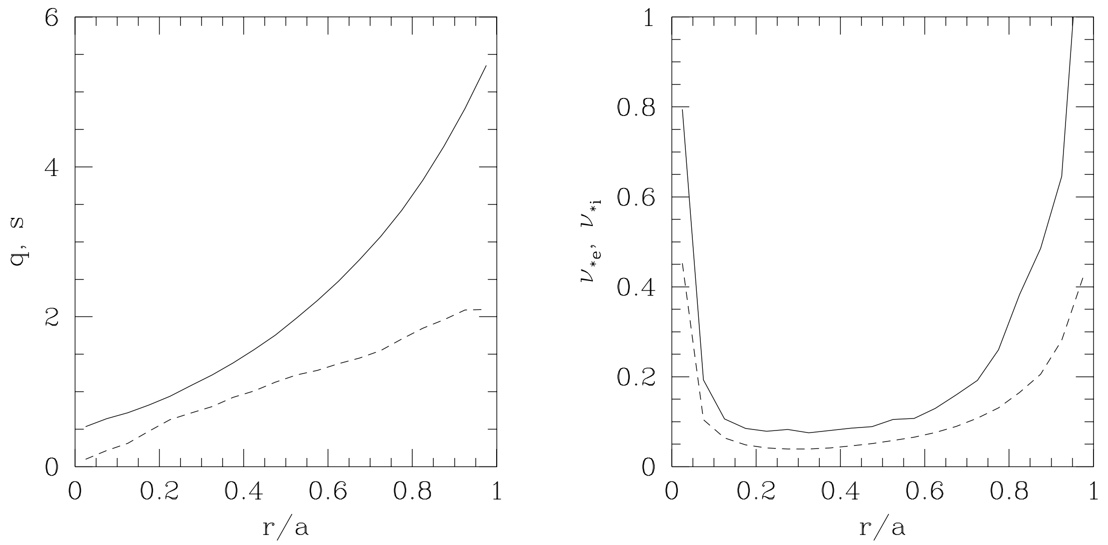

Figure 6.3: Safety factor, q (solid), shear, $\hat{s}$ (dashed), electron (solid) and ion (dashed) collisionality for #65018.

inferred heat flux, Q_i, is fairly smooth. Since $\chi^{\mathrm{PB}} \propto Q_i/\nabla T_i$, if the measured ∇T_i is slightly lower than its actual value, χ^{PB} a will be slightly higher than the actual χ_i. The simulation χ^{sim} is proportional to ∇T_i, since the turbulence here is primarily driven by the ion temperature gradient. Since the simulations use ∇T_i as an input, if ∇T_i is slightly low, χ^{sim} will be low. Therefore, small errors in ∇T_i push χ^{sim} and χ^{PB} in opposite directions. Taking this into account, Fig. 6.4 shows reasonable agreement between the toroidal gyrofluid results and the experimental results in the core region, $r/a < 0.7$, for both χ_i and χ_e. The heat transport is reduced in the core where the toroidal ITG mode is more weakly driven than, for example, at $r/a = 0.5$.

Outside $r/a = 0.7$, the predicted χ_i is clearly too low. There are a few possible explanations which could make the predicted edge transport increase, due to effects which are not included in these simulations. Increased damping of the turbulence-generated sheared flows near the edge would increase the flux (see Fig. 5.5). Increased flow damping could possibly come from collisional friction with impurities or from drag due to charge exchange, although the latter is probably quite weak. Another mechanism which would increase the edge transport is inverted im-

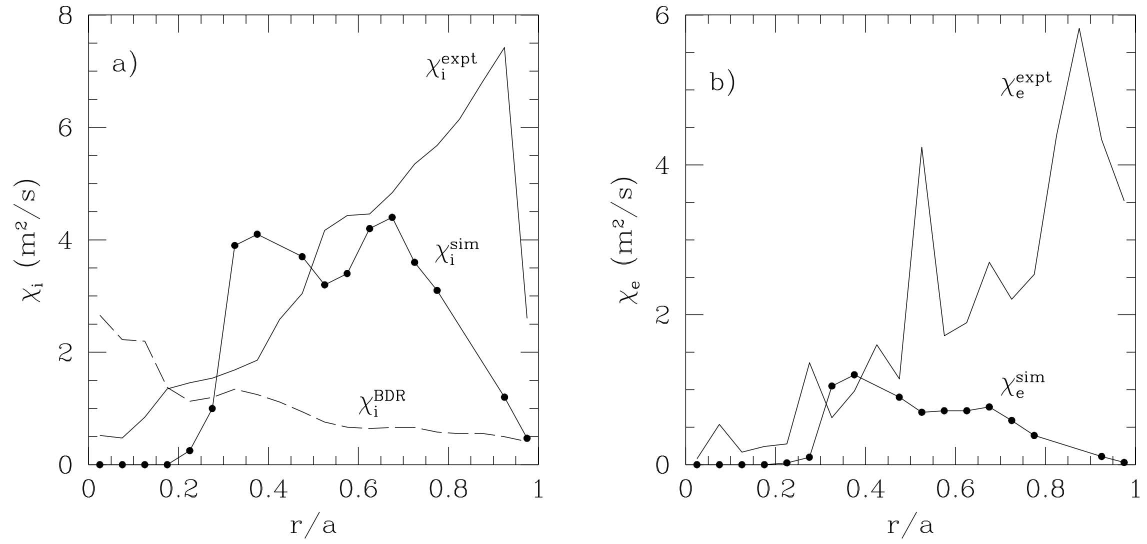

Figure 6.4: (a) Comparison of predicted and experimental $\chi_i(r)$. (b) Comparison of $\chi_e(r)$. The dots are from the simulations and the solid lines without dots are calculated from power balance (SNAP). Also shown is the theoretical χ_i from [Biglari *et al.*, 1989].

purity density gradient drive, as discussed in Section 1.2 [Dorland *et al.*, 1994a]. The radial variation of impurity density is difficult to measure; it is probably easier to find some signature of impurity density gradient driven turbulence in the simulations, and then look for this signature in fluctuation measurements. Another possibility is Kelvin-Helmholtz type drive from sheared equilibrium flows, but it seems unlikely that the flows in the edge are large enough to drive these instabilities. Another possibility is that the large fluctuations at the edge are not generated locally, but are propagating into the edge from more strongly driven core regions [Mattor and Diamond, 1994]. Finally, perhaps some increased drive at the edge could come from the Shafranov shift. Near the edge the flux surfaces are compressed, increasing the local gradient in the bad curvature region. Clearly all these mechanisms are speculative at this point, and should be studied in more detail.

The predicted electron heat flux is in reasonable agreement with experiment in the core, $r/a < 0.5$, but is too low in the edge. In the region $0.5 < r/a < 0.7$, where χ_i matches fairly well, the predicted electron flux may be low due our approximate collision model. As discussed in Section 3.4, we have approximated the velocity dependence of $\nu_e(v)$. Over most of the minor radius, the collisionality for this shot is near $\nu_{\text{eff}} L_n / v_{ti} \approx 1$, where our trapped electron model underestimates the nonadiabatic electron response. (See the right hand side of Fig. 3.5.) Incorporating the velocity dependence of $\nu_e(v)$ could remedy part of this discrepancy.

Overall, this seems to be a reasonable level of agreement. The gyrofluid equations appear to be accurate enough to properly capture the small linear drive in the core, where the plasma is near marginality, without resorting to fully kinetic linear theory. Small changes in ∇T_i and ∇T_e could make the agreement virtually exact for $r/a < 0.7$. To demonstrate this, comparison of this shot with the IFS-PPPL χ_i interpolation formula based on our toroidal gyrofluid simulations with adiabatic electrons and linear fully kinetic calculations is shown in Fig. 6.5(a). This interpolation formula for χ_i found by [Dorland *et al.*, 1994b]:

$$\chi_i = \frac{\rho_i^2 v_{ti}}{R} \left(\frac{R}{L_{Ti}} - \frac{R}{L_{Ti}^{\text{crit}}} \right)^{1,1/2} \mathcal{F}, \tag{6.1}$$

is quite similar to the results with trapped electrons (Fig. 6.4) for this moderate collisionality. In Eq. (6.1), $\mathcal{F} = q/(2 + \hat{s}) \cdots$, is a complicated function of local dimensionless parameters, and R/L_{Ti}^{crit} is determined from kinetic calculations

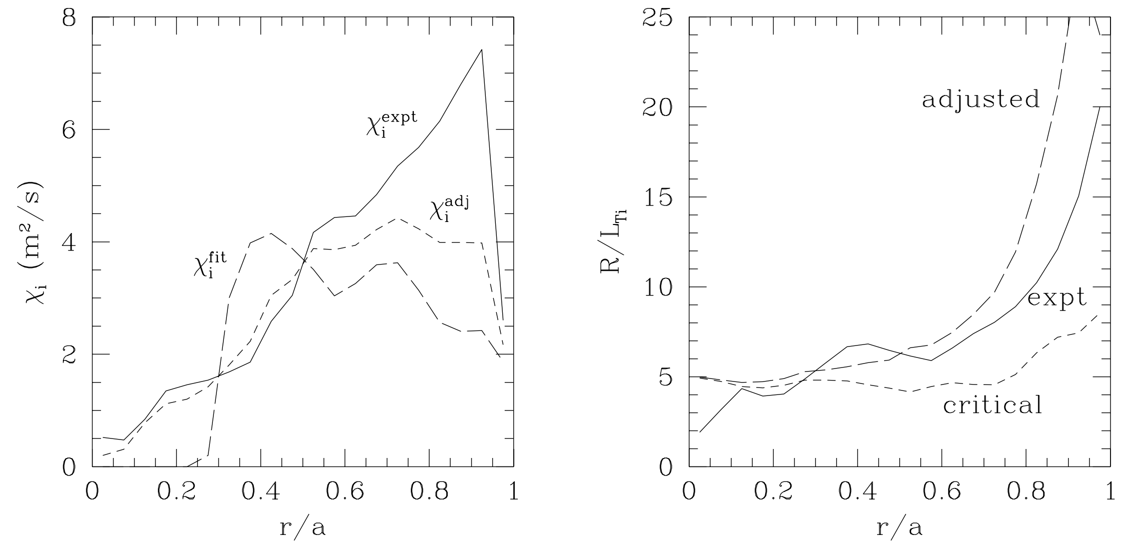

Figure 6.5: (a) Comparison of experimental $\chi_i(r)$ (solid) and and the IFS-PPPL $\chi_i(r)$ (long dashes). Also shown is the IFS-PPPL $\chi_i(r)$ using an $L_{Ti}(r)$ profile adjusted so the predicted heat flux matches the experimental heat flux (short dashes). (b) Measured (solid) and adjusted (long dashes) R/L_{Ti}. In the core, the adjusted R/L_{Ti} is only slightly above the critical R/L_{ti} (short dashes).

[Kotschenreuther *et al.*, 1994b]. If $L_{Ti}(r)$ is adjusted so the predicted heat flux, Q_i, matches the measured heat flux, $\chi_i(r)$ is in much better agreement, as shown by the χ_i^{adj} in Fig. 6.5(a). This is similar to the results which would be obtained from the predictive transport code used in [Dorland *et al.*, 1994b]. Fig. 6.5(b) shows the measured R/L_{Ti}, the adjusted R/L_{Ti}, and R/L_{Ti}^{crit}. The adjusted R/L_{Ti} is only slightly above marginal in the core, since the measured heat flux there is small. Fig. 6.6 shows the T_i profile obtained by integrating the adjusted $L_{Ti}(r)$ inward, using the measured T_i at $r/a = 0.8$ as a boundary condition. Thus, only a relatively small change in $T_i(r)$ is needed to get the predicted χ_i to agree. This is an example of usual marginal stability effects as emphasized again in [Dorland *et al.*, 1994b]. A good sawtooth model might further improve the T_i fit in the core.

This encourages us to add more physics to these simulations to try to explain a wider range of experimental conditions. With nonadiabatic electrons, at sufficiently small ν_{*e}, there is often no rigorous critical L_{Ti} beyond which the modes

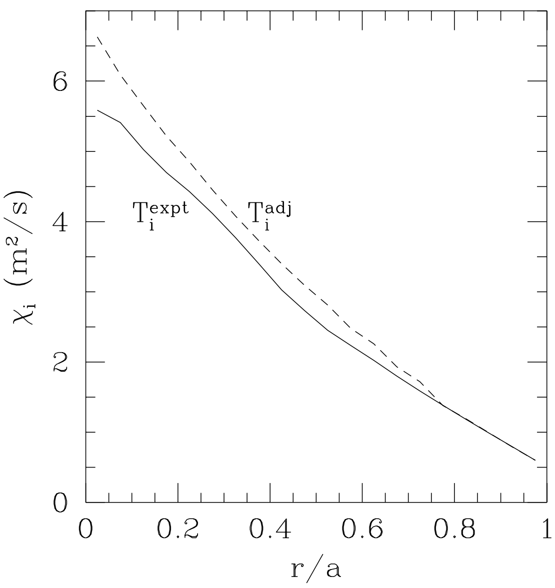

Figure 6.6: T_i profile obtained by integrating the adjusted L_{Ti} inward, using the measured T_i at $r/a = 0.8$ as a boundary condition. Only small changes from the measured T_i profile are necessary to make the heat fluxes agree.

are completely stabilized, but there can still be threshold-like behavior where the modes are weaker. For the moderate ν_{*e} of many of the L-modes looked at in [DORLAND *et al.*, 1994b], there is marginal behavior (as in Fig. 6.4(a)), but at lower ν_{*e} there may still be a fairly strong TEM drive with less marginal features. Mapping out precisely when this happens is now possible with our simulations with trapped electrons, and is important work for the future.

There are many experimental transport scalings which appear to contradict microinstability based theories, especially the scaling with current (I_p), B, and ion mass. There is some evidence, however, that the I_p and B scalings are not inconsistent with our results. The q dependence of Eq. (6.1) can lead to I_p scaling. The detailed comparisons in [KOTSCHENREUTHER *et al.*, 1994a] also compare favorably with the current ramp experiments of [ZARNSTORFF *et al.*, 1991]. Although our simulations and Eq. (6.1) are gyro-Bohm, this gyro-Bohm scaling with B can be partially masked by marginal stability effects, leading to a more Bohm-like behavior, as seen in experiments. While the comparisons discussed in this chapter and in [DORLAND *et al.*, 1994b; KOTSCHENREUTHER *et al.*, 1994a] seem to be on the right track, these issues must be carefully addressed.